Title

Bar-driven evolution and quenching of spiral galaxies in cosmological simulations

Journal

Monthly Notices of the Royal Astronomical Society, 465(3)

ISSN

0035-8711

Authors

Spinoso, Daniele
Bonoli, Silvia
Dotti, Massimo
et al.

Publication Date

2017-03-01

DOI

10.1093/mnras/stw2934

Peer reviewed

Mon. Not. R. Astron. Soc. **000**, 1–13 (0000) Printed 11 July 2016 (MN LATEX style file v2.2)

Bar-driven evolution and quenching of spiral galaxies in cosmological simulations

Daniele Spinoso[1⋆], Silvia Bonoli[2], Massimo Dotti[1,3], Lucio Mayer[4,5], Piero Madau[6] and Jillian Bellovary[7]

[1] *Università degli Studi di Milano-Bicocca, Piazza della Scienza 3, 20126 Milano, Italy*
[2] *Centro de estudios de fisí ca del cosmos de Aragó n, plaza San Juan, 1 planta-2 44001 Teruel, Spain*
[3] *INFN, Sezione di Milano-Bicocca, Piazza della Scienza 3, 20126 Milano, Italy*
[4] *Center for Theoretical Astrophysics and Cosmology, Institute for Computational Science, University of Zurich, Winterthurerstrasse 190, CH-8057 Zurich, Switzerland*
[5] *Kavli Institute for Theoretical Physics, Kohn Hall, University of California, Santa Barbara, CA 93106-4030, USA*
[6] *Department of Astronomy & Astrophysics, University of California, 1156 High Street, Santa Cruz, CA 95064*
[7] *Department of Astrophysics, American Museum of Natural History, Central Park West & 79th St, New York, NY 10024*

11 July 2016

ABSTRACT

We analyse the output of the hi-res cosmological "zoom-in" hydrodynamical simulation Eris*BH* to study self-consistently the formation of a strong stellar bar in a Milky Way-type galaxy and its effect on the galactic structure as well as on the central gas distribution and star formation. The simulation includes radiative cooling, star formation, SN feedback and a central massive black hole wich is undergoing gas accretion and is heating the surroundings via thermal AGN feedback. A large central region in the Eris*BH* disk becomes bar-unstable after $z \sim 1.4$, but a clear bar-like structure starts to grow significantly only after $z \simeq 0.4$, possibly triggered by the interaction with a massive satellite. At $z \simeq 0.1$ the bar stabilizes and reaches its maximum radial extent of $l \approx 2.2$ kpc. As the bar grows, it becomes prone to buckling instability, which we quantify based on the anisotropy of the stellar velocity dispersion. The actual buckling event is observable at $z \simeq 0.1$, resulting in the formation of a boxy-peanut bulge clearly discernible in the edge-on view of the galaxy at $z = 0$. The bar in Eris*BH* does not dissolve during the formation of the bulge but it is long-lived and is strongly non-axisymmetric down to the resolution limit of ~ 100 pc at $z = 0$. During its early growth, the bar exerts a strong torque on the gas within its extent and drives gas inflows that enhance the nuclear star formation on sub-kpc scales. Later on, as the bar reaches its maximum length and strength, the infalling gas is nearly all consumed into stars and, to a lesser extent, accreted onto the central black hole, leaving behind a gas-depleted region within the central ~ 2 kpc. Observations would more likely identify a prominent, large-scale bar at the stage when the galactic central region has already been quenched. Bar-driven quenching may play an important role in disk-dominated galaxies at all redshift. AGN feedback is instrumental in this scenario not because it directly leads to quenching, but because it promotes a strong bar by maintaining a flat rotation curve, suppressing the density of baryons within the central kpc in the early stages of the formation of the galaxy.

Key words: galaxies: bulges - galaxies: kinematics and dynamics - galaxies: formation - galaxies: evolution - galaxies: structure - methods: numerical.

1 INTRODUCTION

Bars are extremely common non axisymmetric features in disk galaxies, occurring in up to $\gtrsim$ 30% of massive ($M_* \gtrsim 10^{9.5}\mathrm{M}_\odot$) spirals in the local Uni-

⋆ d.spinoso@campus.unimib.it

verse (Laurikainen, Salo & Buta 2004; Nair & Abraham 2010; Lee et al. 2012a; Gavazzi et al. 2015a). Bars are considered to play a key role in the evolution of disk galaxies, being able to drive strong inflows of gas towards the central galactic regions (e.g. Sanders & Huntley 1976; Roberts, Huntley & van Albada 1979; Athanassoula 1992) and triggering nuclear star-bursts (e.g. Ho, Filippenko & Sargent 1997; Martinet & Friedli 1997; Hunt & Malkan 1999; Laurikainen, Salo & Buta 2004; Jogee, Scoville & Kenney 2005). Bars are also thought to be responsible for the build-up of the pseudo/disky bulges, whose nearly exponential profiles hints to a disk origin (e.g. Kormendy 2013, for a review). These structures are the most common type of bulges among galaxies in the stellar-mass range $10^{9.5}\mathrm{M}_{\odot} < M_{*} < 10^{10.5}\mathrm{M}_{\odot}$, while classical bulges dominate among more massive systems (e.g. Fisher & Drory 2011). Bars can also be responsible for triggering AGN activity, if a fraction of the inflowing gas can reach the central sub-pc of the galaxy (e.g. Shlosman, Frank & Begelman 1989; Berentzen et al. 1998; Sellwood & Moore 1999; Combes 2000; Querejeta et al. 2015; Fanali et al. 2015).

On longer timescales, the removal of the gas forced towards nuclear regions affects the star formation processes within the bar extent (Cheung et al. 2013; Fanali et al. 2015), contributing to the lowering of the specific star formation rate in the most massive spiral galaxies at low redshift (Cheung et al. 2013; Gavazzi et al. 2015a). In addition to the effect of the bar onto the inter stellar medium (ISM), the dynamical evolution of the bar itself is advocated to be responsible for the boxy/peanut-shaped stellar bulges (B/P bulges hereafter) (see Kormendy 2013; Sellwood 2014, for a review), observed in $\gtrsim 40\%$ of edge on disk galaxies (e.g. Lütticke, Dettman & Pohlan 2000). Together with the high fraction of disky pseudobulges, the frequent occurrence of B/P bulges hints at the fundamental importance of secular evolution in the shaping of the central regions of disk galaxies.

Most of the theoretical studies that support the existence of causal connections between bars and the abovementioned structures/processes are either analytical or based on simulations of isolated galaxies (e.g. Athanassoula 1992; Berentzen et al. 1998; Regan & Teuben 2004; Berentzen et al. 2007; Villa-Vargas, Shlosman & Heller 2010; Kim, Seo & Kim 2012; Cole et al. 2014). Although these kind of simulations are extremely informing about the dynamical effect of bars, cosmological simulations are needed to follow bar formation within the hierarchical growth of galaxies (as discussed in, e.g., Kormendy 2013). Furthermore, most of the simulation literature on bar formation and evolution is based on collisionless simulations. A few works have employed hydrodynamics and star formation, showing interesting differences on important issues such as bar survival and bar-buckling (see e.g. Debattista et al. 2006; Athanassoula, Machado & Rodionov 2013; Athanassoula, Lambert & Dehnen 2005), but none of them has employed modern sub-grid recipes for feedback, which constitute a crucial aspect of recent progress in simulating galaxy formation.

To date only an handful of fully cosmological simulations have achieved the required numerical resolution and included all the physical processes needed to self-consistently produce barred galaxies (e.g. Romano-Díaz et al. 2008; Scannapieco & Athanassoula 2012; Kraljic, Bournaud & Martig 2012; Goz et al. 2014; Bonoli et al. 2016; Fiacconi, Feldmann & Mayer 2015; Okamoto et al. 2015). Among the abovementioned cosmological simulations of barred disk galaxies, Eris*BH* (Bonoli et al. 2016) and Argo (Fiacconi, Feldmann & Mayer 2015) share the highest spatial and mass resolutions[1], but Argo has been evolved only down to $z = 3$, while Eris*BH* has been followed down to $z = 0$, so its properties can be compared directly with the observed properties of well-resolved barred galaxies.

Eris*BH* is a twin simulation of Eris (Guedes et al. 2011), with which it shares initial conditions, resolution and sub-grid physics, but, unlike Eris, it also includes prescriptions for the formation, growth and feedback of supermassive black holes. Both Eris and Eris*BH* reseamble, at $z = 0$, a late-type galaxy such as the Milky Way (Guedes et al. 2011; Bonoli et al. 2016), but while Eris hosts a typical pseudobulge, Eris*BH* features a strong bar and its bulge has a clear boxy-peanut morphology (Bonoli et al. 2016).

The aim of this work is to study the buildup and the evolution of the strong bar seen in Eris*BH* , to learn about the origin of bars and the impact that these structures have in shaping galaxies like our own Milky Way.

The paper is organized as follows. In Section 2 we briefly summarize the properties and main results of the Eris*BH* simulation. In Section 3 we study the buildup of the bar, quantifying its strength and radial extent; we analyze the dynamical properties of the galaxy disk, testing its stability to non-axisymmetric perturbations and looking for resonances between the bar bulk precession and the orbital motions of disk stars; we also analyze the formation of the B/P morphology of the bulge. In Section 4 we show the impact of the bar in depleting gas in and triggering star formation in the central region of the galaxy. Finally, in Section 5 we summarize and discuss our results.

2 THE Eris*BH* SIMULATION

Eris*BH* (Bonoli et al. 2016) is one of the runs in the Eris suite of simulations (Guedes et al. 2011; Mayer 2012; Shen et al. 2012; Bird et al. 2013; Shen et al. 2013; Guedes et al. 2013; Rashkov et al. 2013; Sokolowska et al. 2016) which have been among the first zoom-in cosmological simulations to produce realistic late-type spirals with properties comparable with the Milky Way at $z = 0$. Eris*BH* (Bonoli et al. 2016) inherits its initial condition and most of its features from the first Eris run (Guedes et al. 2011, 2013), from which it differs in that it also includes prescriptions for the formation and accretion of massive black holes (MBHs) and their associated AGN feedback. Here we summarize the main characteristics of Eris and the new sub-grid physics implemented in Eris*BH* . For more details we refer the reader to Guedes et al. (2011) and Bonoli et al. (2016).

[1] The simulations by Kraljic, Bournaud & Martig (2012) have a comparable spatial resolution but a coarser resolution in mass.

Eris was obtained from a zoom-in of a Milky Way-size halo selected within a low-resolution, dark matter-only simulation of a $(90\ \mathrm{Mpc})^3$ volume. This simulation assumed a flat universe with $\Omega_\mathrm{M} = 0.24$, $\Omega_\mathrm{b} = 0.042$, $h_0 = 73\ \mathrm{km\ s^{-1}Mpc^{-1}}$, $n = 1$ and $\sigma_8 = 0.76$ obtained from the WMAP three-year data (Spergel et al. (2007)). The target halo was selected also because of its quiet merger-history (i.e. no major mergers after $z = 3$, where a major merger is defined as an encounter between two haloes whose mass ratio is above 1 : 10). The cosmological evolution of the haloes was simulated from $z = 90$ down to $z = 0$ with the parallel N-body spatially and temporally adaptive tree-SPH code *GASOLINE* Wadsley, Stadel & Quinn (2003).

Within the high-resolution region, the initial dark-matter and gas particles masses were set respectively to $m_\mathrm{DM} = 9.8 \times 10^4 \mathrm{M}_\odot$ and $m_\mathrm{g} = 2 \times 10^4 \mathrm{M}_\odot$. The gravitational softening length was fixed to the value of $\varepsilon_0 = 120$ physical parsec for each particle type from $z = 0$ to $z = 9$ and evolved as $\varepsilon(z) = \varepsilon_0(1 + z)^{-1}$ from $z = 9$ to $z = 90$. Eris*BH* , as the original Eris, includes recipes for Compton and atomic cooling, heating from a UV background and radiative cooling. Energy and metals injection in the interstellar medium due to SNe explosions and stellar feedback are modelled following the recipe of Stinson et al. (2010). No metal-line cooling or metal diffusion were included.

Owing to the high resolution of the simulation we could use a relatively high density-threshold for star formation, i.e. $n_\mathrm{SF} = 5\ \mathrm{atoms/cm^3}$. The combination of SNe feedback and the high density-threshold for star formation produces a realistic clumpy interstellar medium (Guedes et al. 2011) and removes low-angular momentum gas from the simulated disk. The final outcome of Eris*BH* is a Milky Way-size disk galaxy with a low bulge-to-disk (B/D) ratio and a flat rotation curve (with rotation velocity at the solar radius of 190 ± 15 km/s), whose location on the Tully-Fisher, stellar-mass/halo-mass, and stellar velocity dispersion-MBH mass relations is consistent with that of the Milky-Way. Note that at $z > 0.5$ both Eris*BH* and Eris have overly efficient star formation relative to the abundance matching predictions, while they agree with it at $z = 0$. Recent runs in the Eris suite which incorporate both metal-line cooling and stronger SN feedback, do obey abundance matching constrainst at higher redshift but miss a kinematically cold thin disk component at $z = 0$ (Sokolowska et al. (2016); Mayer et al., in preparation).

Eris*BH* includes recipes for the seeding, growth and thermal feedback of MBHs. Growth occurs by both mergers with other MBHs and gas accretion. All the other parameters in this new run were kept identical to those in the original Eris in order to allow a coherent comparison between the two simulations. In Eris*BH* , a MBH seed is placed in every halo that (*i*) does not already host a MBH, (*ii*) is resolved with at least 10^5 particles, and (*iii*) hosts at least 10 gas particles in regions denser than 100 atoms/cc. Only four proto-galaxies in the simulation match the abovementioned conditions before $z \sim 3$ and are thus seeded with a MBH, whose mass is proportional to the size of the high-density gas region. After $z \sim 3$ the gas density becomes generally too low for the seeding process to occur (Bonoli et al. 2016), The four black hole seeds are then allowed to accrete mass following the Bondy-Hoyle-Lyttleton prescription capped at the Eddington limit, as implemented in Bellovary et al. (2010). During the accretion phase it is assumed that a small fraction $\epsilon_\mathrm{f} = 0.05$ of the total AGN luminosity couples with the surrounding gas and heats it. The growth of the black hole hosted by the central galaxy is mostly due to mergers with black holes hosted by infalling satellite galaxies, while growth by gas accretion is very modest, as reflected by the low accretion rates measured, typically between 10^{-3} and $10^{-5}\ \mathrm{M_\odot/yr}$ (i.e. only $10^{-2} - 10^{-4}$ of the Eddington limit) (an exhaustive and extended discussion on the growth of the black holes in ErisBH can be found in Bonoli et al. 2016). Despite the limited gas growth, the modest feedback energy released by the central black hole still manages to affect the large-scale properties of the host galaxy. For example, Eris*BH* features a smaller bulge and a more extended disk when compared to Eris. Because of the absence of a prominent central mass concentration, the disk in Eris*BH* is prone to dynamical instabilities during late evolutionary stages (e.g. Kormendy 2013, and references therein) and a clear stellar bar develops within the central $\sim$3 kpc of the disk. A qualitative analysis of the stellar surface density field in late evolutionary stages of Eris*BH* can easily point out the presence of a central non-axisymmetric feature, i.e. a stellar bar (see the lower-left panel of figure 10 in Bonoli et al. 2016, and Figure 1 below for a zoom-in of the central galactic regions).

In the next sections we focus on studying the properties of such bar and its effect on the host galaxy.

3 BAR FORMATION AND EVOLUTION

In this section we first focus on the analysis of the buildup of the bar of Eris*BH* , by quantifying its strength and spatial extent across time. We then study the dynamical stability of the galactic disk, to determine the conditions that led to the developement of the bar. Finally, we study the emergence of the B/P morphology of the bulge and connect it to the growth of the bar.

3.1 Properties of the bar

In order to quantitatively assess the bar extent and strength we perform a Fourier decomposition of the projected stellar density field $\Sigma_*(x; y)$ on the disk plane, by calculating the *cumulative* A_2 amplitude (as in Dubinski, Berentzen & Shlosman 2009; Fiacconi, Feldmann & Mayer 2015):

$$A_2(r) = \frac{1}{M} \sum_{j=1}^{N} m_j \ e^{2i\,\phi_j} \,, \tag{1}$$

where the summation is carried over the entire set of $N = N(r)$ star particlesup to a distance r from the centre and M is the total mass within the same distance. Due to its definition, $A_2(r)$ increases up to the distance at which the $\Sigma(x; y)$ field structure exhibits a strong non-axisymmetric component and then gradually falls to zero. The radial position r_A2 of the maximum value $\mathrm{m_{A2}} = \max[A_2(r)]$ is used as an estimate of the bar radial extent. At the same time, the value of $\mathrm{m_{A2}}$ itself can be used as an estimate of the bar strength, as it measures the bar intensity with respect to the mean projected density field up to $r = r_\mathrm{A2}$.

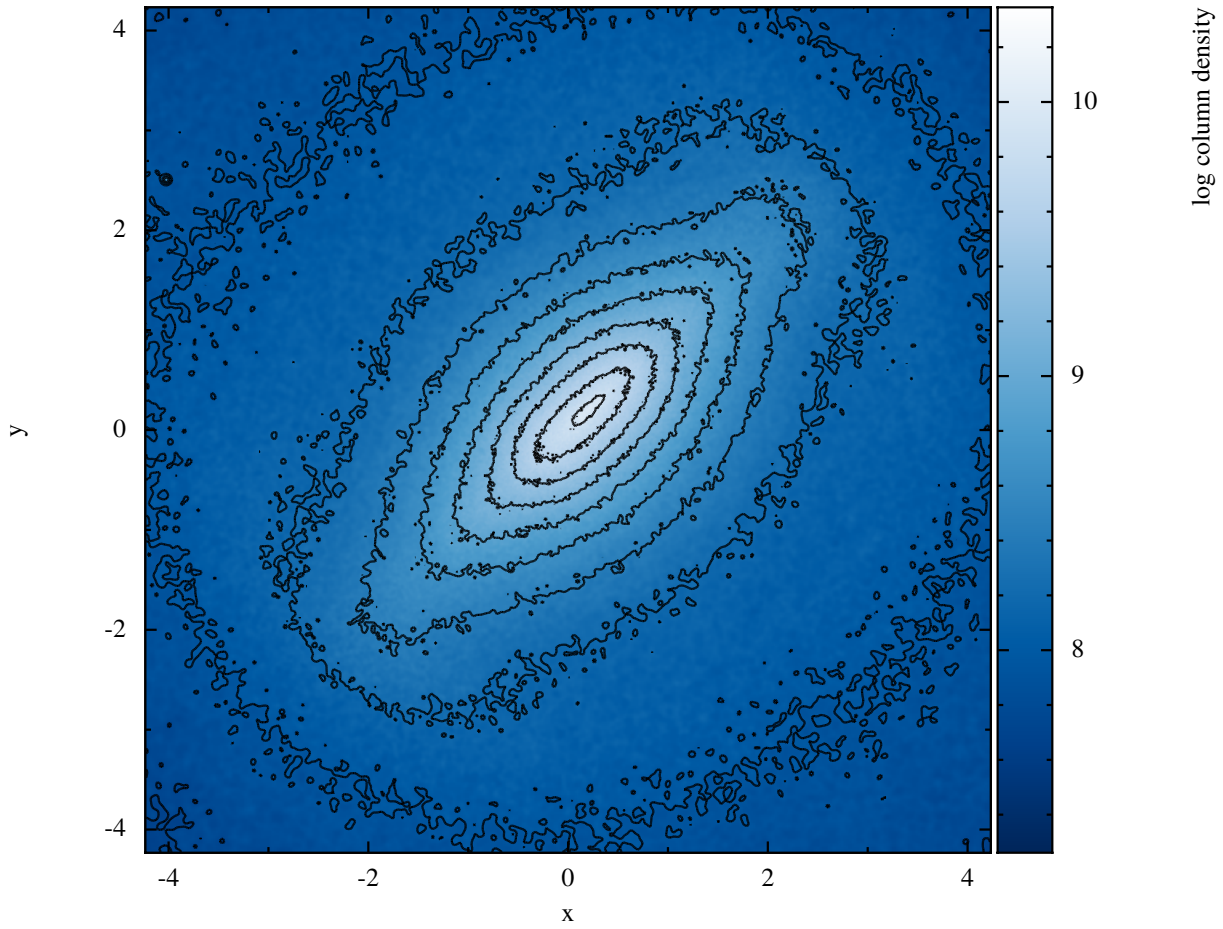

Figure 1. Stellar surface density Σ_* map of the central region of the Eris*BH* galaxy at redshift $z = 0$. The x and y axis units are in [kpc h^{-1}] while the color shades show the values of $\log(\Sigma_*/M_\odot \mathrm{kpc}^{-2})$. The black solid lines are the iso-density contours used to reveal the inner structure of the bar and to show that the non-axisymmetric shape is maintained even at very small radius. Contours are separated by a 0.2 difference in $\log(\Sigma_*)$ starting from a value of $\log(\Sigma_*/M_\odot \mathrm{kpc}^{-2}) = 9.8$ in the centre. Note that the deviation from axisymmetry increases at smaller and smaller radii so that the central bar structure is more elongated than the global bar structure. This feature is common in all the snapshots where the bar is clearly visible.

We calculate the $A_2(r)$ radial profile at each snapshot in order to trace the bar amplitude evolution as well as its radial extent evolution through time (Figure 2). During the early stages of disk formation strong fluctuations in m_{A2} are due to ongoing minor merger events and/or the associated galaxy relaxation events. The last minor merger occurs at $z \sim 1.2$, after which the galaxy evolves pratically in isolation.

From $z \sim 0.5$ and onwards, the intensity of m_{A2} gradually increases with time and reaches its maximum $m_{\mathrm{A2}} \approx 0.27$ close to the end of the simulation. Results in Figure 2 show that the bar radial extent reaches its maximum value $r_{\mathrm{max}} \approx 2.2$ kpc at late simulation stages. The bar extent stabilizes about $r \approx 2.1$ kpc after $z \lesssim 0.1$, in correspondence with the growth of a central B/P bulge (see below). The bar strength and the formation time we measure in ErisBH are consistent with previously published results obtained from both isolated and cosmological simulations (e.g. Kraljic, Bournaud & Martig 2012; Cole et al. 2014; Fiacconi, Feldmann & Mayer 2015; Polyachenko, Berczik & Just 2016), although we note that a large scatter in particular in the growth time (from $\lesssim 1$ Gyr to $\gtrsim 3$ Gyr for Milky Way like galaxies) is present in literature.

3.2 Dynamical stability of the galactic disk

The absence of a central massive bulge makes the galaxy naturally unstable to the growth of a bar as soon as it settles in a dynamically cold rotationally supported structure. For $z < 1.5$ the disk dynamical properties allow for the amplification of density perturbations through the *swing amplification effect* (see e.g. Binney & Tremaine 2008) which may easily promote the growth of a bar-like structure. The effectiveness of this process is linked to both the Toomre parameter Q and the swing amplification parameter X (see e.g. Toomre 1964; Goldreich & Tremaine 1978, 1979). For a differentially-rotating stellar disk the two parameters are defined as (see e.g. Binney & Tremaine 2008)

$$Q(R) = \frac{\sigma_r(R), \kappa(R)}{3.36\, G\Sigma(R)} \; ; \quad X(R) = \frac{R\, \kappa^2(R)}{4\, \pi\, G\Sigma(R)} \qquad (2)$$

where $\sigma_r(R)$ is the radial velocity dispersion of the stars, $\kappa(R)$ is the epicyclic frequency, G is the gravitational con-

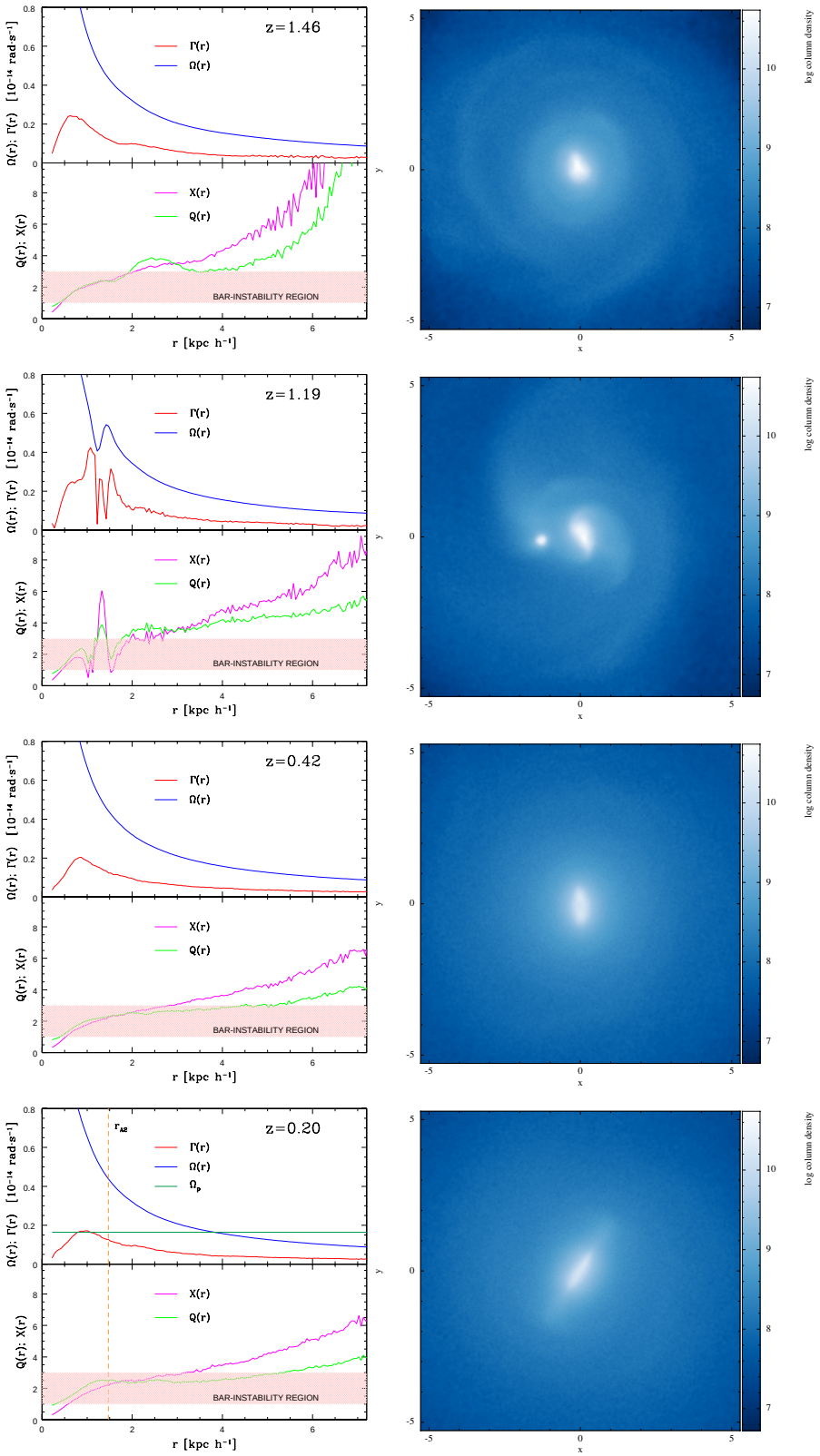

Figure 3. Dynamical and morphological structure of the main galaxies at different evolutionary stages. From top to bottom: before ($z = 1.46$), during ($z = 1.19$) and after ($z = 0.42$ and $z = 0.20$) the occurrence of the last minor merger. Left panels: frequency plots (Ω and Γ, upper half) and Q and X stability parameters as a function of the radius. The red-shaded area highlights the bar instability region ($1 \lesssim Q \lesssim 2$ and $1 \lesssim X \lesssim 3$) in each panel. The orange vertical dashed line in the bottom panel marks the bar extent, while the horizontal green line refers to the bar rotation frequency. Right panels: face-on projection of the stellar density map at the corresponding redshifts. Colors encode the stellar surface density (in units of $M_\odot$ kpc^{-2}) on a logarithmic scale. The merging companion is clearly visible in the second panel from the top.

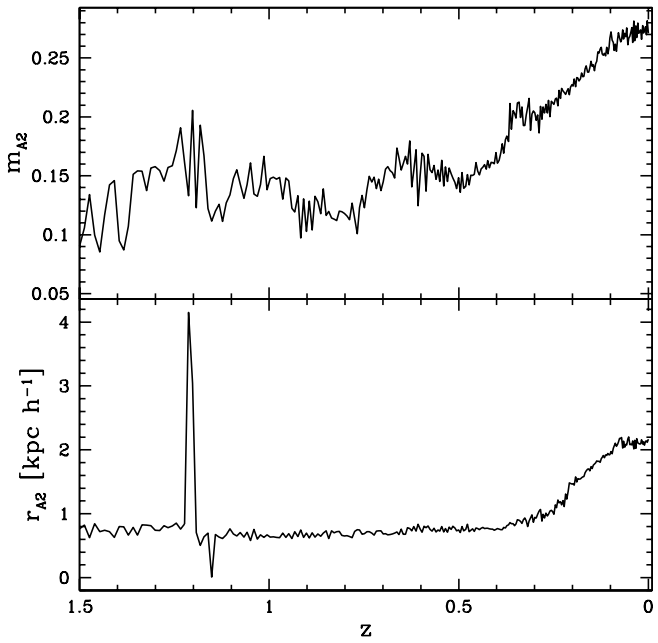

Figure 2. Evolution with redshift of m_{A2} (upper panel) and r_{A2} (lower panel). The early fluctuation at $z \approx 1.2$ is caused by the last minor merger experienced by the main galaxy. A clear transition towards constantly increasing values of m_{A2} and r_{A2} is observable at $z \lesssim 0.5$, associated with the growth of the galactic bar. A flattening in the m_{A2} and r_{A2} profiles is observable at low redshift $z \lesssim 0.1$ in correspondance of the boxy-peanut bulge formation, as discussed in the following.

stant and $\Sigma(R)$ is the star surface density. The Toomre parameter accounts for the disk stability to axisymmetric density perturbations: if $Q \leqslant 1$ the disk is unstable. On the other hand the swing amplification parameter X quantifies whether non-axisymmetric perturbations can grow. Two conditions must be simultaneously verified for the swing amplification to be effective: $Q \gtrsim 1$ so that the disk is stable but still strongly responsive to density perturbations, and $X \lesssim 3$ to prevent the density waves from being too tightly wound (see Binney & Tremaine 2008).

Figure 3 shows the Q and X radial profiles calculated at four different times. As the two parameters are in the range $1 \lesssim Q \lesssim 2$ and $1 \lesssim X \lesssim 3$ (figure 3, red-shaded areas in left panels), it is clear that an extended central region (i.e. up to $r \sim 3$ kpc) is prone to bar instability. For reference, the face-on view of the stellar surface density map of the galaxy is shown in the right panels. The effect of the minor merger happening at $z \approx 1.2$ on stellar dynamics is clearly observable both in the Q and X profiles (that show local peaks at the location of the satellite), as well as in the frequency plot, showing both the angular velocity Ω and the precessional frequency $\Gamma = \Omega - \kappa/2$, where κ is the epicyclic frequency. This merger imprints a degree of non-axisymmetry on the central stellar distribution. It is however unclear whether the merger-driven asymmetric structure is the seed of the stellar bar observable at lower redshifts or not. Because of the noisy evolution of the m_{A2} parameter at $z \gtrsim 0.5$ it is impossible to firmly assert that the bar starts growing already at $z \approx 0.8$ (1.5 Gyr after the completion of the merger) or only at $z \approx 0.5$ (about 3.5 Gyr after the merger). For such reason we refrain from commenting further on the trigger of the bar instability in this section. A discussion about possible future investigations designed to answer this particular question is presented in the conclusions.

The angular frequency ($\Omega_{\rm bar}$) and extent of the bar are shown in the lower left panel of Figure 3 (horizontal green and vertical red lines, respectively). The bar rotates with a frequency of ≈ 30 km s^{-1} kpc^{-1} at $z = 0$ wich is similar to the frequency estimated for the Milky Way (Gerhard 2011) and approximately equal to the maximum of $\Gamma(R)$. This is somewhat expected, since perturbations with $\Omega_{\rm bar} \approx \max(\Gamma)$ are the fastest to grow, as demonstrated for the first time by Sanders (1977). The lack of a clear Inner Lindblad resonance (ILR, defined by the equivalence $\Omega_{\rm bar} = \Gamma(R_{\rm ILR})$), of the kind of those observable in presence of a strong central concentration of matter (where Γ tends to diverge for small radii) maintains the elongated bar like structure even at small (sub-kpc) radii (see figure 1). The consequences of the absence of a clear ILRs on the fate of the bar-perturbed gas will be discussed in the next section.

It is also evident that the bar does not extend out to its corotational radius ($R_{\rm cor}$ defined by the $\Omega_{\rm bar} = \Omega(R)$ equality), but stops at considerably smaller radii ($r_{A2} \sim 0.5 R_{\rm cor}$), in agreement with the results of previously published cosmological (e.g. Okamoto et al. 2015) as well as in idealized simulations of tidally induced bars (e.g. Lokas et al. 2016). We stress however that the $r_{A2}/R_{\rm cor}$ ratio we found is considerably smaller than that of most of the observed bars(e.g. Aguerri et al. 2015, and references therein), although some galaxies host bars whose $r_{A2}/R_{\rm cor}$ ratios are consistent with the ones we find (Rautiainen et al. 2008). On a theoretical ground, small $r_{A2}/R_{\rm cor}$ ratios have been predicted both for bars triggered by interactions (Miwa & Noguchi 1998) possibly like the one discussed here and for bars growing in galaxies with an initially low bulge to disk mass ratio (Combes & Elmegreen 1993), as it is the case of the Eris*BH* simulation.

3.3 The emergence of the B/P morphology of the bulge

As already commented, the bar stops growing when a B/P structure starts to form in the central region of the disk. The B/P feature can be easily pointed out by a qualitative edge-on view analysis of the Eris*BH* latest evolutionary stages (see Bonoli et al. 2016, and Figure 4). To constrain the time evolution of the B/P structure we perform a quantitative analysis on the edge-on projected density field at each snapshot. We first select the $(x; y)$ plane defined by the bar major axis and the direction perpendicular to the disk plane. On such plane we measure the $|z|^+(x)$ and $|z|^-(x)$ locations of the median value of the Σ_* above or below the disk plane as a function of the x position (as in Iannuzi & Athanassoula 2015). Figure 5 shows an example of the $|z|^{\pm}(x)$ behaviour with respect to the x coordinate at redshift $z = 0$.

A double-horned shape is clearly observable in the $|z|^+(x)$ and $|z|^-(x)$ profiles. To study the growth in time of the B/P bulge, we first calculate two reference values z_0^+ and z_0^- on the $|z|^+$ and $|z|^-$ profiles respectively, by averaging $|z|^+$ and $|z|^-$ in the intervals $x \in [-4; -3]$ and $x \in [3; 4]$ (outside the bar region, in the unperturbed disk, see the blue

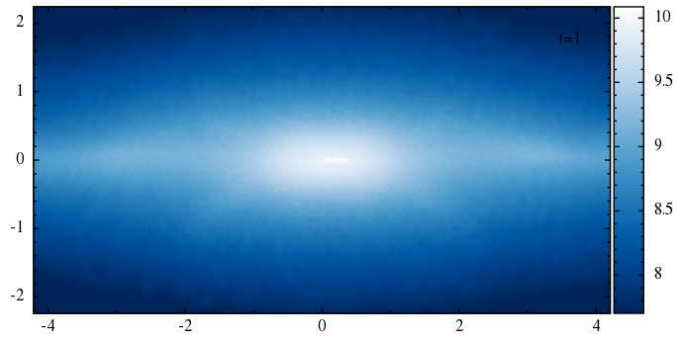

Figure 4. Edge-on view of the Eris*BH* last snapshot (redshift $z = 0$) in which the boxy-peanut shape is clearly visible. The bar major axis is perpendicular to the line of sight to enhance the visibility of the boxy-peanut structure. Units are the same as in figures 1 and 3.

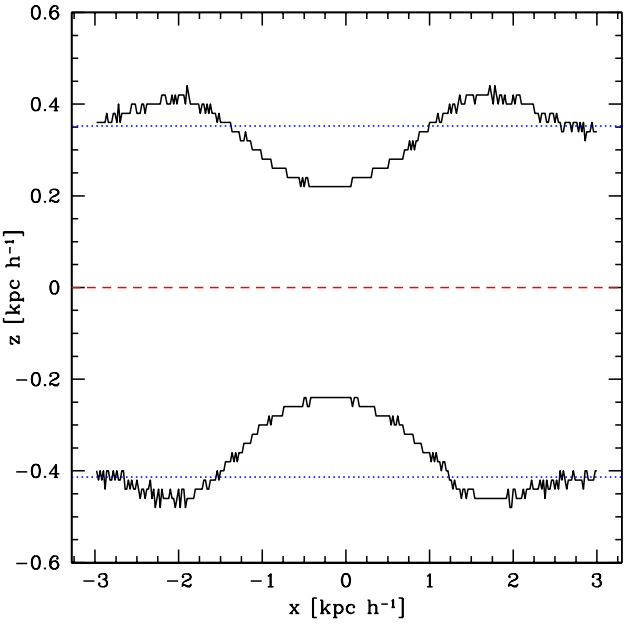

Figure 5. $|z|^+$ and $|z|^-$ profiles (red dashed lines) with respect to the x coordinate, computed above and under the disk plane, respectively, at redshift $z = 0$. A double-horned feature is evident in both profiles, demonstrating the presence of a boxy-peanut structure in the central region of the galaxy (Iannuzi & Athanassoula 2015). The dashed horizontal red line marks the position of the galactic plane in the $(x; z)$ plane. The blue dotted lines are reference lines used to calculate the relative intensity of the peaks in the $|z|^+$ and $|z|^-$ profiles (see text).

dotted lines in Figure 5). This reference value is then used to measure the quantity

$$h = \max[\,|z|\,] - z_0 \tag{3}$$

on the four quadrants of the disk projection, and the average of the four values $h_{\rm m}$ is compared with $\sigma_r = \max[\sigma^+; \sigma^-]$ where σ^+ and σ^- are the standard deviations of the $|z|^+$ and $|z|^-$ profiles around the reference values z_0^+ and z_0^- in the outer disk[2]. If no double-horned feature is present in the $|z|^{\pm}(x)$ profiles, then $h_{\rm m}$ must be comparable to σ_r. The results of this analysis are shown in the upper panel of Figure 6. Clearly $h_{\rm m}(z)$ becomes consistently bigger than σ_r only after redshift $z \simeq 0.1$, i.e. the double-horned feature (and so the B/P structure in the bulge) develops at late evolutionary stages, when the bar is already strong, as shown by the $r_{\rm A2}$ evolution (shown for $z \lesssim 0.4$ in the lower panel of Figure 6 for any easy comparison). In order to constrain the origin of the B/P bulge we computed the parameter $\mathrm{B} = (\sigma_z/\sigma_{\rm x})^2$ within the central 3 kpc of the disk, where σ_z and σ_x are the vertical and radial velocity dispersions measured on a slit along the bar major axis. As discussed in Martinez-Valpuesta, Shlosman & Heller (2006) (and references therein), $\mathrm{B} \lesssim 0.3$ corresponds to a buckling unstable galactic nucleus. As expected, B decreases in time after the formation of the bar, because of the rise of σ_x, down to the buckling unstable regime. As soon as the B/P bulge forms B rises again, because of the increase in σ_z associated with the buckling event. The buckling nature of the B/P structure is still observable in the asymmetric (with respect to the equatorial plane) mass distribution of the $z = 0$ disk (see Figure 4). We note that $r_{\rm A2}$ stops growing when the B/P structure forms and grows, consistently with the scenario of bars-weakening proposed by, e.g., Combes & Sanders (1981); Sellwod & Wilkinson (1993); Kormendy (2013).

4 GAS RESPONSE TO THE BAR GROWTH AND CONSEQUENCES ON STAR FORMATION

In this section we focus on the impact that the bar has on the evolution of the gas and stellar component of the galaxy in the region dominated by the bar.

4.1 Gravitational torque and gas evolution

As the bar grows and gains strength, it starts exherting torques on the gas component of the galaxy, modifying completely its distribution in the central region. In Figure 7 we show the surface density of the gas at four different epochs. The central region (approximately within 3 kpc from the centre) of the galaxy at $z = 0$ appears almost empty of gas, except for an unresolved density peak in the galactic nucleus. The quantitative evolution of the gas content in the galaxy center is shown in figure 8, where we show the surface density profile of the gas at different times. In this case we renormalize the profiles in the unperturbed region of the galaxy ($4 \lesssim R \lesssim 10$ kpc). This allows to emphasize the effect of the bar, averaging out the effects of cosmological gas accretion and star formation-related gas consumption on large scales.

Figures 7 and 8 clearly show the torquing effect that the growing bar has onto the gas. The gas within the bar extent

[2] We take the maximum between σ^+ and σ^- to be more conservative

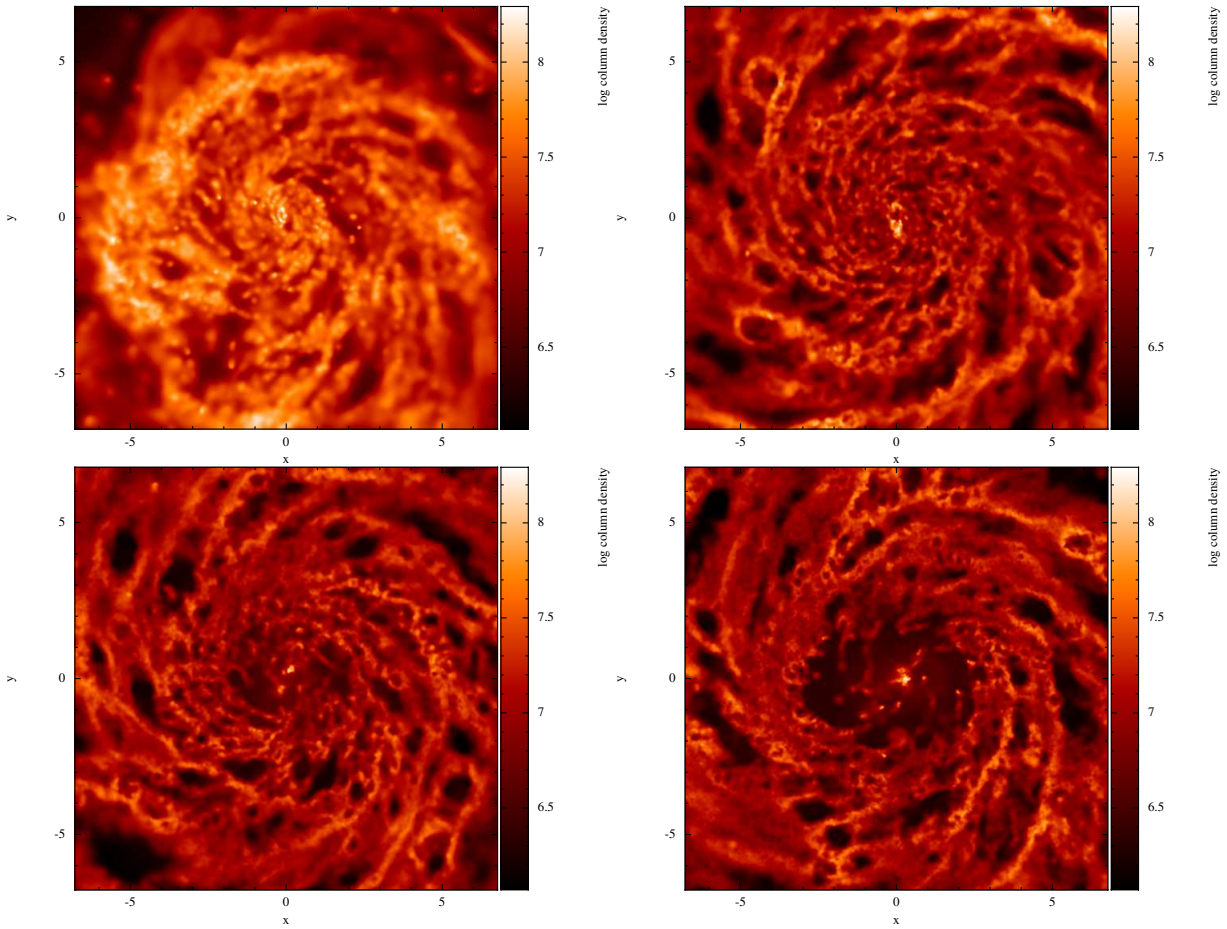

Figure 7. Map of the gas surface density at four different epochs, $z = 1.46$, $z = 0.42$, $z = 0.20$ and at the end of the simulation $z = 0$ (upper left, upper right, lower left and lower right panel, respectively). Units are the same as in figures 1, 3 and 4 but we plot the gas surface density in a red color-scale.

is driven towards the centre of the galaxy[3], and the majority of it is converted in stars (see below). Because of the absence of a clear ILR the gas does not settle into a nuclear ring of star formation, but keeps on being torqued by the bar down to the very central region of the galaxy, where it forms an unresolved clump surrounded by a region completely depleated of gas (see the bottom-right panel of Figure 7). To confirm this picture we estimate the relevance of the torque that the stellar distribution exert onto the gas. Following Mundell & Shone (1999) and Emsellem et al. (2015) we calculate the strength of the torque using:

$$Q_{\rm t}(r) = \frac{\max\left[\frac{1}{r}\frac{\partial\phi(r;\theta)}{\partial\theta}\right]}{\left\langle\frac{\partial\phi(r;\theta)}{\partial r}\right\rangle_{\theta}} \qquad (4)$$

which, if, effectively, the ratio between the maximum tangential force and the mean axisymmetric force at each radius r. The maximum value of $Q_{\rm t}$ can also be used to classify the bar strength, with $\max(Q_{\rm t}) > 0.4$ corresponding to structures hosting strong bars (e.g. Buta, Laurikainen & Salo 2004; Buta et al. 2005). The torque profile at $z = 0$ is shown in Figure 9. The maximum value of $Q_{\rm t}$ is $Q_{\rm t} \approx 0.56$, confirming the strong bar nature of the central non-axisymmetric structure. More interestingly, the curve is peaked at very small radii close to our resolution limit, which explains the formation of a compact central gas overdensity and is consistent with the highly non-axisymmetric distribution of the stars at the smallest radii (see Figure 1). The bar does persists until $z = 0$, thus most of the stellar mass in the inner 1-2 kpc remains associated with the bar rather than growing further the small pseudobulge. This is consistent with the notion that large central masses (of the order of a tenth of the total stellar disk) within a very compact size (well within one thenth of the disk scale length), are needed to destroy the bar (see e.g. Shen & Sellwood 2004) while here the central overdensity is modest (about 3 % of the total stellar mass within 300 pc), without any clear nuclear overdensity present.

We calculated the $Q_{\rm t}(r)$ profiles at different times to sample the bar strength evolution with respect to time. We find that the maximum torque is always obtained near the galaxy centre (i.e. up to $r \simeq 250$ pc), confirming that the bar in Eris*BH* can be very effective in changing the gas an-

[3] We checked that the gas outflow from the central region is negligible by calculating the total mass in star and gas within the bar final extent ($r = 2.17$ kpc) with respect to redshift during the bar growth phase. We find that the total baryonic mass is conserved within $\sim 3\%$ of its value at $z \sim 0.45$ (before bar formation), thus excluding strong inflows/outflows of material.

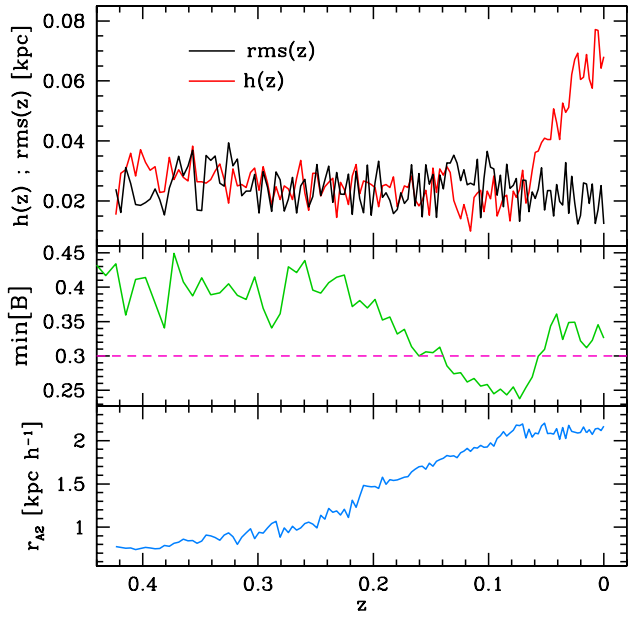

Figure 6. Upper panel: B/P strength as a function of redshift z. The red line refers to the relative height h of the $|z|(x)$ peak to a reference value z_0, while the error on the z_0 average σ_r is shown in black. Middle panel: minimim value of the parameter $B = (\sigma_z/\sigma_x)^2$ within the inner 3 kpc from the main galaxy centre, as a function of redshift. The bar is buckling unstable for $B \lesssim 0.3$. Lower panel: evolution of the bar length r_{A2} in the same redshift interval. Note that $h(z)$ becomes consistently bigger than σ_r towards the end of the simulation (upper panel), when the bar stops increasing its size and strength (lower panel).

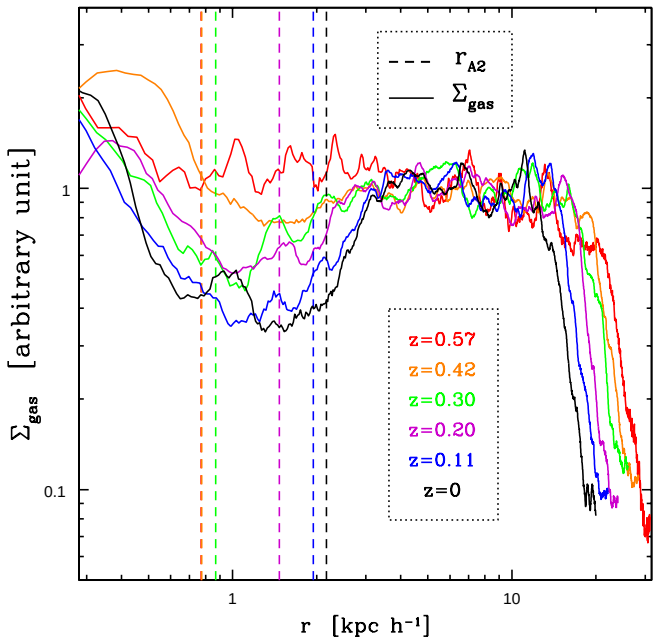

Figure 8. Gas surface density profile at different times. The dashed vertical lines show the bar extent at the different times. Note that the surface densities has been renormalized to minimize the differences among the different profiles in the $4 \lesssim R \lesssim 10$ region.

gular momentum up to the very smallest radii and make it fall towards the centre. This means that the bar can efficiently feed the central region, providing the fuel necessary to ignite later evolutionary phenomena such as nuclear star formation (e.g. Kormendy (2013) and AGN activity (e.g. Combes 2000; Querejeta et al. 2015). In ErisBH , however, the accretion of matter onto the central MBH at low z is very modest (Bonoli et al. 2016). Most of the matter inflowing towards sub-kpc scales during the formation of the bar reaches densities large enough to be turned into stars (within a region of ~ 600 pc), where nuclear star formation then becomes the dominant process, as we discuss below.

4.2 Star formation and black hole accretion

The strong central gas inflows caused by the torques exherted by the growing bar, naturally lead to changes in the star formation and nuclear activity of the galaxy. Bonoli et al. (2016) already showed that the star formation rate and the black hole accretion rate increase after $z \sim 0.2$, which is when the bar is reaching maximum strength (see Figure 2). We further quantify the effect of the gas inflow onto the central star formation and nuclear activity here. In Figure 10 (upper panel) we show the radial distributions of young stars (with an age < 0.6 Gyr, i.e. formed after $z \approx 0.05$) and those formed after the build-up of the bar structure at $z \approx 0.4$ (i.e. those with an age < 4.5 Gyr). The ratio between these two quantities (bottom panel) clearly

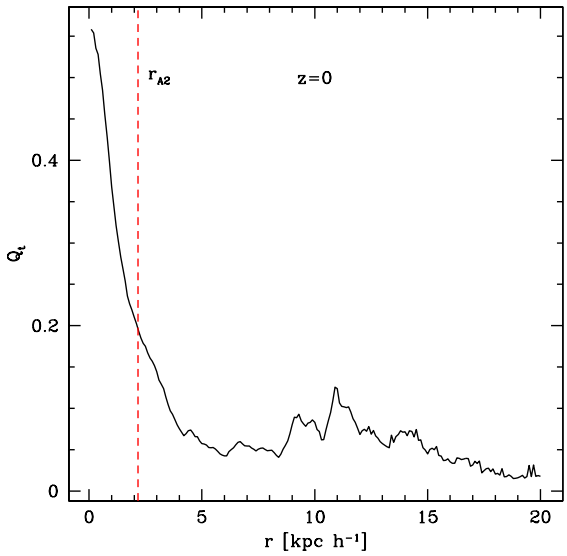

Figure 9. Radial profile of $Q_t(r)$ at $z = 0$ (black curve). The size of the bar (r_{A2}) at the same redshift is indicated by the red dashed line for reference. We see clearly a high central value ($Q_m = 0.56$ at $r \simeq 0.15$ kpc) and no relative maximum at $r \simeq r_{A2}$. It is remarkable that the profile monotonically decreases up to $r \simeq 4$ kpc from the centre. This shows that the bar non-axisymmetric structure is very coherent and the bar does not "dissolve" into a spherical bulge at small radii. This implies also the possibility that the bar efficiently drives the gas inflow up to the very central region of the disk.

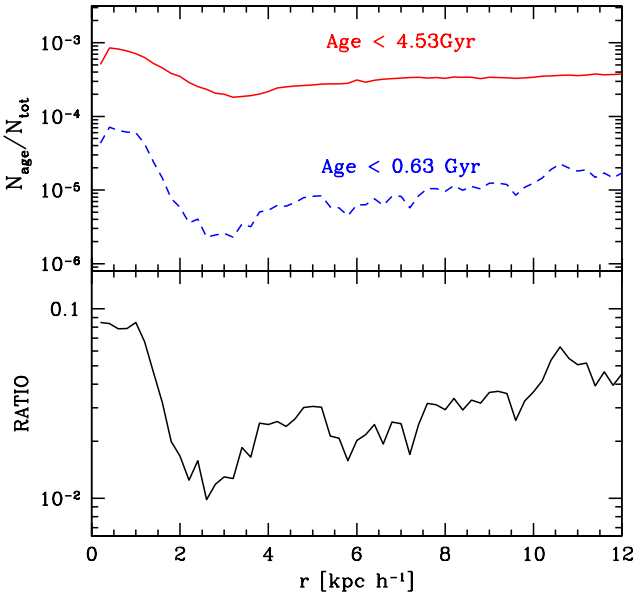

Figure 10. Upper panel: radial distribution at $z = 0$ of young stars formed after $z \approx 0.05$ (i.e. with an age < 0.6 Gyr, blue dashed line) and stars formed after the bar build-up at $z \approx 0.4$ (with an age < 4.5 Gyr, red solid line). The ratio of these two quantities (bottom panel) shows the signatures of a recent star formation episode (within ~ 1 kpc) which transformed into stars the gas torqued down by the bar gravitational effect. This produced a gas-poor "dead zone" between $2 \lesssim r \lesssim 3$ kpc (see also figure 7 bottom-right panel) where a low number of young stars is present.

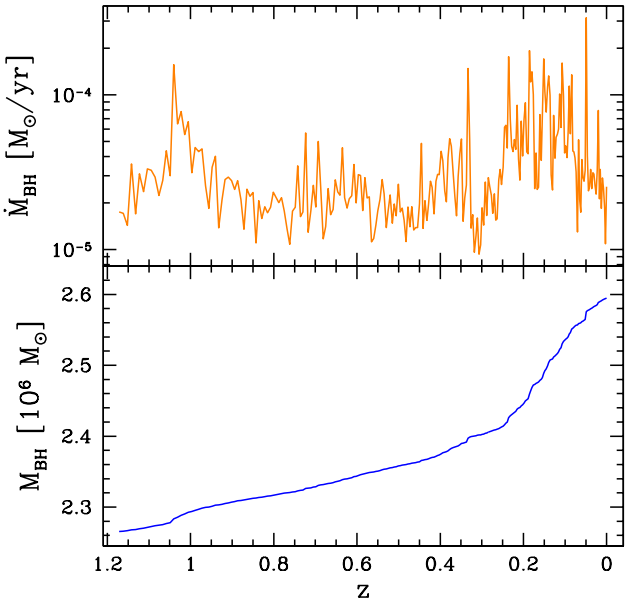

Figure 11. Accretion rate (upper panel) and mass evolution (lower panel) of the central black hole with respect to time. $\dot{M}_\odot$ is generally low confirming that the BH mass growth by gas accretion is very small after the last minor merger (about $\sim 14\%$ of its final value). An increase in the MBH accretion rate is observable during the development of the bar structure but $\dot{M}_\odot$ remains modest even after $z \sim 0.3$.

points out the presence of a recent star formation episode in the very central region of the galaxy (i.e. within ≈ 1 kpc).

A fraction of the inflowing gas gets accreted by the MBH. Figure 11 (upper panel) shows the black hole accretion rate as a function of redshift from the last minor merger to $z = 0$. $\dot{M}_\odot$ is generally very low, fluctuating about $2 \times 10^{-5} \mathrm{M}_\odot \mathrm{yr}^{-1}$ with the exception of some isolated spikes (see also Bonoli et al. 2016). This implies a modest growth of the black hole mass after $z \sim 1.2$, which undergoes a total increment of about $\sim 14\%$ of its final value (lower panel). A slight change in the accretion regime can be observed during the bar growth phase for $z \lesssim 0.3$. The accretion rate results, however, in a luminosity lower than $\sim 1\%$ of the MBH Eddington limit, assuming a radiative efficiency of $\eta = 0.1$. This further support the picture in which the gas within the reach of the bar torques falls into the centre of the galaxy and is promptly consumed by nuclear star formation bursts, while only a very small fraction of it fuels the nuclear accretion process. As the gas infall proceeds all the way to the center it leaves behind a low gas density region, a "dead zone‘ visible in at 400 pc - 2 kpc in Figure 8, within which star formation can not be further sustained (Cheung et al. 2013; Gavazzi et al. 2015a; Fanali et al. 2015). The bar in ErisBH does not extend out to its corotational radius (see Fig 3), i.e. its precession period is shorter than the orbital period of the outer gas. As a consequence the bar exerts a positive torque onto the outer gas, preventing any further gas infall that could potentially replenish the dead zone.

On the contrary, the formation of new stars proceeds unimpeded outside the region affected by the bar. To further support this picture figure 12 shows the density weighted map of the stellar ages at the end of the simulation. A population of young stars is clearly visible in the outer regions of the galaxy, while only old stars are present in the dead region. A nuclear ($\lesssim 1$ kpc), elongated structure with intermediate age stars is visible at the centre of the galaxy, in which the stars forming at the bar onset contribute to the average age. A qualitative comparison with the similar structure of NGC 1073 is shown in figure 12. The outer disk in NGC 1073 is mostly composed of star formation regions which host young stellar populations. On the contrary, a bar structure is evident in the galaxy centre where the almost-exclusive presence of old and red stars is a prominent feature.

5 CONCLUSIONS

We analyzed the high-resolution cosmological Eris*BH* run (Bonoli et al. 2016), which closely resembles an Sb/Sc galaxy with stellar mass and rotation velocity comparable to our Milky Way. At $z = 0$ the galaxy forming at the centre of the refined region features a strong nuclear ($R \approx 2$ kpc) bar which is able to strongly influence: (*i*) the dynamics of the stellar disk, including the formation of a B/P bulge in its centre; (*ii*) the dynamics of the gas within the central 3 kpc, which falls towards the galactic centre triggering a short burst of star formation in the galactic nucleus (within ~ 600 pc) as soon as the bar starts growing; (*iii*) the late star formation in the central ~ 3 kpc. This is the consequence

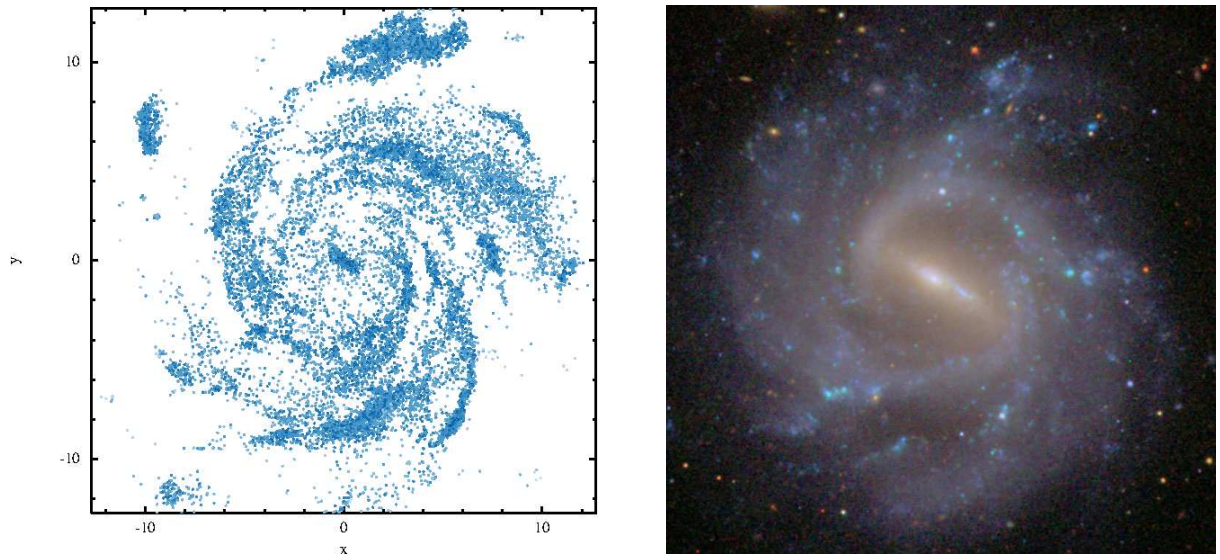

Figure 12. Left panel: distribution at redshift $z = 0$ of the youngest stars, i.e. those with an age < 35 Myr (formed at $z \approx 0.0026$, well after the bar build-up). The outer regions of the disk are populated with young stars while a "dead region" in which few young stars are present is clearly visible in the central region (i.e. up to ~ 2 kpc from the centre). The dead region hosts a central bar-like distribution of young stars. Right panel: the disk galaxy NGC 1073 is shown for a qualitative comparison. The outer regions of the NGC 1073 disk show star formation regions which host young stellar populations while the inner regions exhibit a complex structure of older stars similar to that in Eris*BH* .

of the fast gas removal operated by the bar preventing any strong star formation episode after its formation.

The analysis of the torques operated by the bar supports the notion that the bar efficiently drives gas inflows down to the resolution limit ($\sim$ hundreds of pc, due to the absence of any clear ILR) at any $z \lesssim 0.4$. The absence of an intense star formation activity in the central regions of the disk as well as of strong AGN activity is purely due to the absence of dense gas within the bar extent due to rapid consumption by star formation at the onset of bar formation. The lack of a clear observational correlation between AGN activity and the occurrence of bars in galaxies (see e.g. Ho, Filippenko & Sargent 1997; Mulchaey & Regan 1997; Hunt & Malkan 1999; Knapen, Shlosman & Peletier 2000; Laine et al. 2002; Lee et al. 2012b; Alonso, Coldwell & Lambas 2013; Cisternas et al. 2013; Cheung et al. 2015, for the different point of views) could be related to the prompt removal of gas. If we assume the results of Eris*BH* appy to the whole class of field disk galaxies in low density environments, we argue that the stronger gas inflow and enahnced star formation happen at the onset of bar formation, when the detection of a bar is more difficult as the bar is shorter and less regular in shape. Instead, when the bar is stronger and well-developed, hence easily determined from photometry or imaging, star formation has already ceased creating a "dead zone" in the galactic centre and making the occurrence of any nuclear activity less probable (see e.g. the discussion in Fanali et al. 2015).

Strong bars may arise at earlier times in more massive galaxies or galaxies living in dense environments, which evolve on shorter dynamical timescales. Hence we argue that bar formation can contribute to quenching and the formation of "red nuggets" at $z > 1$, as also suggested by the results of the ARGO simulations which exhibit several example of early bar formation leading to increased central baryonic densities (Fiacconi, Feldmann & Mayer 2015). Bar-driven quenching should thus be seen as an alternative to mergers, disk fragmentation into massive clumps and AGN feedback, the main mechanisms explored in the literature over the last few years. Of course bar-driven quenching is related to feedback mechanisms operating in the central region, as it seems to be the case in Eris*BH* where AGN feedback might be instrumental in creating favourable conditions for bar formation at later stages. Since bar-formation requires a kinematically cold, thin disk to occur, it remains to be seen if this can be achieved by the latest generation of strong feedback models adopted in galaxy formation simulations.

It is interesting to note that such a strong bar is absent in the Eris run, which differs from Eris*BH* only because it does not feature any MBH accretion and feedback prescription. This would seem to be at odd with the limited gas accretion occurring onto the central MBH (Bonoli et al. 2016), that would imply a moderate effect of AGN feedback onto the host galaxy. However, at $z > 1$ there are transient near-Eddington accretion phases which ought to have an effect on the build-up of the central baryonic distribution. Indeed at $z < 1$ Eris*BH* has a much flatter rotation curve near the center as a result of the suppressed growth of the central baryonic density.

The actual trigger of bar growth is still to be pinpointed. The main galaxy in the Eris*BH* run becomes bar unstable at large redshift (see Figure 3), but the bar structure forms only after the last minor merger episode. As discussed in section 3, the properties of the bar do resemble those predicted for a tidally induced one. Whether the merger itself does provide the trigger for the instability to grow is unclear, as it is impossible to definitively constrain the time in between the merger and the actual onset of the bar growth.

In order to test the possible tidal nature of the bar we plan to run a set of simulations restarting the Eris*BH* run before the merger, removing the particles forming the satellite, and checking whether the bar grows regardless of the perturbation.

In conclusion, the present analysis of the Eris*BH* run has demonstrated that a bar resulting from the fully cosmological evolution of adisk galaxy with quiet merger history strongly affects its host, in particular by quenching its star formation on kpc scales. This result provides further theoretical support to the recent claim by Gavazzi et al. (2015a) that bars are one of the main contributor of the flattening observed at high masses in the star formation rate-stellar mass correlation (Whitaker et al. 2012; Magnelli et al. 2014; Whitaker et al. 2014; Gavazzi et al. 2015b; Ilbert et al. 2015; Lee et al. 2015; Schreiber et al. 2016).

ACKNOWLEDGMENTS

The Authors acknowledge Lia Athanassoula, Guido Consolandi, Victor de Battista, Luca Graziani & Giuseppe Gavazzi for the insightful comments and suggestions. Figures 1, 3 (right panels), 4, 7 and 12 (left panel) were produced using the SPLASH visualization tool for SPH data (Price 2007).

REFERENCES

Agertz O., Teyssier R. & Moore B., 2011, MNRAS, 410, 1391
Aguerri, J. A. L., Méndez-Abreu, J., Falcón-Barroso, J., et al. 2015, A&A, 576, A102
Ahn C. P., Alexandroff R., Prieto C. A., et al., 2014, AJ, 211, 17
Alonso M. S., Coldwell G., Lambas D. G., 2013, A&A, 549, A141
Athanassoula E., 1992, MNRAS, 259, 345
Athanassoula E., Machado E. G. & Rodionov S. A., 2013, MNRAS, 429, 1949
Athanassoula E., Lambert J. C. & Dehnen W., 2005, MNRAS, 363, 496
Binney J. & Tremaine S., 2008, "Galactic Dynamics", 2nd Edition, Princeton University: Princeton University Press
Bellovary J. M., Governato F., Quinn T. R., Wadsley J., Shen S., Volonteri M., 2010, ApJ, 721, L148
Berentzen I., Heller C. H., Shlosman I., Fricke K. J., 1998, MNRAS, 300, 49
Berentzen I., Shlosman I., Martinez-Valpuesta I., Heller C. H., 2007, ApJ, 666, 189
Bird J. C., Kazantzidis S., Weinberg D. H., Guedes J., Callegari S., Mayer L. & Madau P., 2013, ApJ, 773, 43
Bondi H., 1952, MNRAS, 112, 195
Bondi H. & Hoyle F., 1944, MNRAS, 104, 273
Bonoli S., Mayer L. , Kazantzidis S., Madau P., Bellovary J., & Governato F., 2016, MNRAS, 459, 2603
Buta R., Laurikainen E., & Salo H., 2004, AJ, 127, 279
Buta R., Vasylyev S., Salo H., & Laurikainen E., 2005, AJ, 130, 506
Cheung E. et al., 2013, ApJ, 779, 162
Cheung E. et al., 2015, MNRAS, 447, 506
Cisternas M. et al., 2013, ApJ, 776, 50
Cole D. R., Debattista V. P., Erwin P., Earp S. W. F., Roškar R., 2014, MNRAS, 445, 3352
Combes, F., & Elmegreen, B. G. 1993, A&A, 271, 391
Combes F., 2000, arXiv:astro-ph/0010570v1
Combes F. & Sanders R. H., 1981, A & A, 96, 164
Contopoulos G., 1980, A & A 81, 198
Debattista V. P., Mayer L., Carollo M. C., Moore B., Wadsley J. & Quinn T., 2006, ApJ, 645, 209
Dubinski J., Berentzen I., & Shlosman I., 2009, ApJ, 697, 293
Emsellem E., Renaud F., Bournaud F., Elmegreen B., Combes F. & Gabor J. M., 2015, MNRAS, 446, 2468
Fanali R., Dotti M., Fiacconi D. & Haardt F., 2015, MNRAS, 454, 3641
Fiacconi D., Feldmann R. & Mayer L., 2015, MNRAS, 446, 1957 Sanders & Huntley (1976), Combes & Sanders (1981),
Fisher D. B. & Drory N., 2011, ApJ, 733, L47
Gavazzi G. et al., 2015a, A&A, 580, A116
Gavazzi G., Consolandi G., Viscardi E. et al. 2015b, A&A, 576, A16
Gerhard O. 2011, Mem. Soc. Astron. Ital. Suppl., 18, 185
Goldreich P., & Tremaine S. 1978, ApJ, 222, 850
Goldreich, P. & Tremaine S. 1979, ApJ, 233, 857
Governato F., Brook C., Mayer L., Brooks A., Rhee G., Wadsley J., Jonsson P., Willman B., Stinson G., Quinn T. & Madau P., 2010, arXiv:0911.2237v1
Goz D., Monaco P., Murante G., Curir A., 2014, [arXiv:1412.2883]
Guedes J., Callegari S., Madau P. & Mayer L., 2011, ApJ, 742, 76
Guedes J., Mayer L., Carollo M. C. & Madau P. 2013, ApJ, 772, 36
Ho L. C., Filippenko A. V., Sargent W. L. W., 1997, ApJ, 487, 591
Hoyle F. & Lyttleton R. A., 1939, in Proceedings of the Cambridge Philosophical Society Vol. 35 of Proceedings of the Cambridge Philosophical Society, The effect of interstellar matter on climatic variation. pp 405
Hunt L. K., Malkan M. A., 1999, ApJ, 516, 660
Iannuzzi F. & Athanassoula E., 2015, MNRAS, 450, 2514
Ilbert, O., Arnouts, S., Le Floc'h, E., et al. 2015, A&A, 579, A2
Jogee S., Scoville N., Kenney J. D. P., 2005, ApJ, 630, 837
Kim W.-T., Seo W.-Y., Kim Y., 2012, ApJ, 758, 14
Knapen J. H., Shlosman I., Peletier R. F., 2000, ApJ, 529, 93
Kormendy J., 2013, Secular Evolution of Galaxies, 1, [arXiv:1311.2609v1]
Kraljic K., Bournaud F., Martig M., 2012, ApJ, 757, 60
Laine S., Shlosman I., Knapen J. H., Peletier R. F., 2002, ApJ, 567, 97
Laurikainen E., Salo H., Buta R., 2004, ApJ, 607, 103
Lee G.-H., Park C., Lee M. G., Choi Y.-Y., 2012a, ApJ, 745, 125
Lee G.-H., Woo J.-H., Lee M. G., Hwang H. S., Lee J. C., Sohn J., Lee J. H., 2012b, ApJ, 750, 141
Lee, N., Sanders, D. B., Casey, C. M., et al. 2015, ApJ, 801, 80
Lokas E. L., Ebrova I., del Pino A., et al. submitted to ApJ

[arXiv:1601.07433]
Lütticke R., Dettman R.-J. & Pholen M., 2000, A&A, 362, 435
Magnelli, B., Lutz, D., Saintonge, A., et al., 2014, A&A, 561, A86
Martinet L., Friedli D., 1997, A&A, 323, 363
Martinez-Valpuesta I., Shlosman I., Heller C., 2006, ApJ, 637, 214
Mayer L., 2012, ASPCS, 453, 289
Miwa, T., & Noguchi, M. 1998, ApJ, 499, 149
Mulchaey J. S., Regan M. W., 1997, ApJ, 482, L135
Mundell C. G. & Shone D. L., 1999, MNRAS, 304, 475
Nair P. B., Abraham R. G., 2010, ApJ, 714, L260
Okamoto T., Isoe M., & Habe A. 2015, PASJ, 67, 63
Ostriker J. P. & Peebles P. J. E., 1973, ApJ, 186, 467
Price D. J. 2007, Publications of the Astronomical Society of Australia, 24, 159
Polyachenko E. V., Berczik P. & Just A., 2016, submitted to MNRAS (arXiv:1601.06115v1)
Querejeta M., Meidt S., Schinnerer E., García-Burillo S., Dobbs C., Colombo D., Dumas G., Hughes A., Kramer C., Leroy A., Pety J., Schuster K. & Thompson T., 2015, submitted to A & A (arXiv:1510.03440v1)
Rashkov V., Pillepich A., Deason A. J., Madau P., Rockosi C. M., Guedes J. & Mayer L., 2013, ApJ, 773, L32
Rautiainen, P., Salo, H., & Laurikainen, E. 2008, MNRAS, 388, 1803
Regan M. W., Teuben P. J., 2004, ApJ, 600, 595
Roberts, Jr. W. W., Huntley J. M., van Albada G. D., 1979, ApJ, 233, 67
Romano-Díaz E., Shlosman I., Heller C., Hoffman Y., 2008, ApJ, 687, L13
Sanders R. H., 1977, ApJ, 217, 916
Sanders R. H. & Huntley J. M., 1976, ApJ, 209, 53
Scannapieco C., Athanassoula E., 2012, MNRAS, 425, L10
Schreiber, C., Pannella, M., Elbaz, D., et al. 2015, A&A, 575, A74
Schreiber, C., Elbaz, D., Pannella, M., et al. 2016, arXiv:1601.04226
Sellwood J. A., 2014, Reviews of Modern Physics, 86, 1
Sellwood J. A. & Wilkinson A., 1993, RPP, 56, 173
Sellwood J. A. & Moore E. M., 1999, ApJ, 510, 125
Shen S., Madau P., Aguirre A., Guedes J., Mayer L. & Wadsley J. 2012, ApJ, 760, 50
Shen S., Madau P., Guedes J., Mayer L., Prochaska J. X. & Wadsley J. 2013, ApJ, 765, 89
Shen S. & Sellwood J. A. 2004, AAS, 36, 1551
Shlosman I., Frank J., Begelman M. C., 1989, Nature, 338, 45
Spergel D. N., Bean R., Doré O., Nolta M. R., Bennett C. L., Dunkley J., Hinshaw G., Jarosik N., Komatsu E., Page L., Peiris H. V., Verde L., Halpern M., Hill R. S., Kogut A., Limon M., Meyer S. S., Odegard N., Tucker G. S., Weiland J. L., Wollack E., & Wright E. L., 2007, ApJ, 170, 377
Sokolowska A., Mayer L., Babul A., Madau P. & Shen S., 2016, ApJ, 819, 1
Stinson G. S., Bailin J., Couchman H., Wadsley J., Shen S., Nickerson S., Brook C. & Quinn T., 2010, MNRAS, 408, 812
Toomre, A. 1964, ApJ, 139, 1217
Villa-Vargas J., Shlosman I., Heller C., 2010, ApJ, 719, 1470
Wadsley J.W., Stadel J. & Quinn T., 2003, arXiv:astro-ph/0303521v1
Whitaker, K. E., van Dokkum, P. G., Brammer, G., & Franx, M. 2012, ApJ, 754, L29
Whitaker, K. E., Franx, M., Leja, J., et al. 2014, ApJ, 795, 104

This paper has been typeset from a TEX/ LATEX file prepared by the author.